Les Cahiers du GERAD ISSN: 0711–2440

High-order simulation of geological units at the Saramacca gold deposit, Suriname

D. Morales, R. Dimitrakopoulos

G–2021–20

April 2021

La publication de ces rapports de recherche est rendue possible grâce au soutien de HEC Montréal, Polytechnique Montréal, Université McGill, Université du Québec à Montréal, ainsi que du Fonds de recherche du Québec – Nature et technologies.

Dépôt légal – Bibliothèque et Archives nationales du Québec, 2021
– Bibliothèque et Archives Canada, 2021

The publication of these research reports is made possible thanks to the support of HEC Montréal, Polytechnique Montréal, McGill University, Université du Québec à Montréal, as well as the Fonds de recherche du Québec – Nature et technologies.

Legal deposit – Bibliothèque et Archives nationales du Québec, 2021
– Library and Archives Canada, 2021

GERAD HEC Montréal
3000, chemin de la Côte-Sainte-Catherine
Montréal (Québec) Canada H3T 2A7

Tél. : 514 340-6053
Téléc. : 514 340-5665
info@gerad.ca
www.gerad.ca

High-order simulation of geological units at the Saramacca gold deposit, Suriname

Daniel Morales [a, b, c]

Roussos Dimitrakopoulos [a, b, c]

[a] *GERAD, Montréal (Qc), Canada, H3T 1J4*

[b] *COSMO – Stochastic Mine Planning Laboratory, McGill University, Montréal (Qc), Canada, H3A 2A7*

[c] *Department of Mining and Materials Engineering, McGill University, Montréal (Qc), Canada, H3A 2A7*

daniel.morales2@mcgill.ca
roussos.dimitrakopoulos@mcgill.ca

April 2021
Les Cahiers du GERAD
G–2021–20

Abstract : Geostatistically simulated representations of mineral deposits are used for resource/reserve assessments, mine design and production planning, project evaluation and so on. Categorical simulation methods are part of the related framework and are used to generate realizations of geological units and their boundaries. The simulation of the geological units of a gold deposit is presented in this paper, based on a data-driven, high-order geostatistical simulation method. The latter method makes neither distributional assumptions nor utilizes a training image, but consistently uses high-order spatial statistics from the available data. The application at the Saramacca gold deposit, Suriname, shows the practical aspects of the method, including the validation of simulated realizations of geological units through the reproduction of the high-order statistics of the data.

Keywords : Categorical geostatistical simulation, high-order simulation, Saramacca gold deposit

1 Introduction

Geological units correspond to different types of material found in a mineral deposit. These geological units have different distributions in space and affect several aspects of deposit modeling, tonnage-grade curves and evaluations, while also affecting mine design, planning and production scheduling. The mathematical modelling of geological units with a single wireframe has been proposed in the past based on implicit functions methods (Mallet 1988 ; Caumon et al. 2013 ; Renaudeau et al. 2019). These methods automate the wireframing process to generate smooth surface representations that do not account for the variability and uncertainty of boundaries between geological units. Stochastic simulation methods for geological units have been developed to account for the uncertainty and variability of geological boundaries, including the sequential indicator simulation method (Journel 1983), which makes no assumption of the underlying probability distributions, but is based on two-point statistics that do not capture complex spatial-geological patterns. Truncated Gaussian (Matheron et al. 1987) and PluriGaussian methods (Galli et al. 1994) are also based on two-point statistics and assume Gaussian distributions.

With the aim of reproducing complex spatial patterns, multiple point simulation methods (MPS) were introduced (Guardiano and Srivastava 1993 ; Strebelle 2002, 2012 ; Krishnan and Journel 2003 ; Journel 2005 ; Remy et al. 2009 ; Mariethoz et al. 2010 ; Mariethoz and Caers 2014). These MPS methods rely not only on the available samples, but also on a training image (TI) from which spatial patterns are obtained. Typically, simulated realizations using MPS methods reproduce the patterns and statistics from the TI. However, when substantial drilling information is available, such a in the case of mineral deposits mined, the TI patterns and related spatial statistics may conflict with the statistics of the available sample data (Osterholt and Dimitrakopoulos 2007 ; Goodfellow et al. 2012).

High-order simulation methods (HOSIM) for continuous and categorical variables have been proposed as a generalization of second-order simulation methods (Dimitrakopoulos et al. 2010 ; Mustapha and Dimitrakopoulos 2010b, 2010a, 2011 ; Minniakhmetov and Dimitrakopoulos 2017a, 2017b, 2018, 2021 ; Yao et al. 2018). HOSIM not only overcomes any distributional assumption, similarly to MPS approaches, but it also provides explicit mathematical approaches for inferring related probability distributions. For this, HOSIM uses high-order spatial cumulants (or moments) to obtain complex curvilinear geologic patterns, while taking in account their connectivity.

For continuous variables, the use of cumulants are described as combinations of moments of statistical parameters by Dimitrakopoulos et al. (2010). A data driven simulation method for continuous variables was proposed by Mustapha and Dimitrakopoulos (2010a) where a conditional probability density function (*cpdf*) is approximated by Legendre polynomials. These developments are advanced by Minniakhmetov et al (2017a) based on the introduction of Legendre-like orthogonal splines. For categorical variables, cumulants and Legendre polynomials are replaced by moments and splines respectively by Mustapha and Dimitrakopoulos (2010a). High-order statistics are computed by high-order spatial indicator moments of data and are approximated through splines which allows inference. High-order spatial indicator moments are consistently connected in their different orders through boundary conditions, which provides the relation that lower orders are embedded in higher order spatial indicator moments. As data statistics are consistently honored in their different orders, realizations are data-driven rather than TI-driven, as in MPS methods. The method does not require the use of external information from a TI, but it can still be included as an option.

The present work demonstrates a detailed of the HOSIM method proposed by Minniakhmetov and Dimitrakopoulos (2021) at the Saramacca gold deposit in Surinam, where four geological units of interest are considered. In the following sections, the HOSIM method utilized is first outlined. Subsequently, the application of the method at the Saramacca gold deposit is detailed, including the validation of the simulated realizations of the deposit. Conclusions and future work follow.

2 Method

The high-order categorical simulation method applied to the Saramacca gold deposit was introduced by Minniakhmetov and Dimitrakopoulos (2021) and is summarized in this section.

2.1 High-order spatial indicator simulation

Let (Ω, F, P) be a probability space. Consider the stationary ergodic random field $\mathbf{Z} = (Z_1, Z_2, \ldots, Z_G)^T, Z : \Omega \rightarrow S^G$ defined on a grid $D = \{\mathbf{x}_1, \mathbf{x}_2, \ldots, \mathbf{x}_G\}$, $\mathbf{x} \in \mathbb{R}^m, m = 2, 3$, such that $Z(\mathbf{x}_i) = Z_i, i = 1, \ldots, G$. The space of all possible outcomes corresponds to Ω, F contains all combinations of Ω, and P is the probability measure. For example, the probability for a given random variable Z_1, $p_{Z_1}(z_1) = P(Z_1 = k_1)$. S^G is a set of states represented by categories $k, k = 1, .., K$. The high-order simulation method provides realizations of $\mathbf{Z}$ for all nodes of a grid D. Lower case z stands for outcome of random variable Z.

High-order categorical simulation method is based on the concept of sequential simulation, where the multivariate distribution $p_{\mathbf{z}}(\mathbf{z})$ can be decomposed into the product of univariate conditional distribution functions

$$\begin{aligned} p_{\mathbf{Z}}\left(\mathbf{z}\middle|d^1\right) =& p_{\mathbf{Z}}\left(z_1, z_2, \ldots, z_G\middle|d^1\right) \\ =& p_{Z_1}\left(z_1\middle|d^1\right) \cdot p_{Z_2}\left(z_2\middle|d^2\right) \cdot \cdots p_{Z_N}\left(z_N\middle|d^G\right). \end{aligned} \tag{1}$$

Here $d^1 = \{d_n\}, d^i = d^{i-1} \cup \{Z_{i-1}\}$, $i = 1, \ldots, G$, and $d_n = \{z_\alpha,\ \alpha = 1, \ldots, n\}$ which represents the set of initial conditioning data.

In practice, instead of considering all the points for each location, only the data and simulated points inside a local neighborhood are used. Without loss of generality, for location $\mathbf{x}_0$, the neighborhood $\Lambda^0 \subseteq d^0$ is be used (Dimitrakopoulos and Luo, 2004) :

$$p_{Z_0}\left(z_0\middle|d^0\right) \approx p_{Z_0}\left(z_0\middle|\Lambda^0\right). \tag{2}$$

Conditional distribution in Equation (2) can be computed by

$$p_{Z_0}\left(z_0\middle|\Lambda^0\right) = \frac{p_{\mathbf{Z}}(\mathbf{z})}{p_{\mathbf{Z}_0^c}\left(\mathbf{z}_0^c\right)}, \tag{3}$$

where superscript c represents the complement of a field with respect the variable given by the subscript 0; for which $\mathbf{Z}_0^c = \mathbf{Z} \backslash Z_0$ and $\mathbf{z}_0^c = \mathbf{z} \backslash z_0$ are obtained. Denominator $p_{\mathbf{Z}_0^c}(\mathbf{z}_0^c)$ is the normalization coefficient

$$p_{\mathbf{Z}_0^c}\left(\mathbf{z}_0^c\right) = \sum_{k_0=1}^{K} P\left(Z_0 = k_0,\ Z_1 = k_1, \ldots, Z_n = k_n\right). \tag{4}$$

The joint distribution $p_{\mathbf{Z}}(\mathbf{z})$ is obtained through high-order spatial indicator moments, described in the next subsection.

2.2 High-order spatial indicator moments

The joint distribution $p_{\mathbf{Z}}(\mathbf{z})$ is equivalent to the spatial indicator moment M (Vargas-Guzman 2011)

$$P\left(Z_{i_1} = k_1, Z_{i_2} = k_2, \ldots\right) = E\left(I_{k_1}\left(Z_{i_1}\right), I_{k_2}\left(Z_{i_2}\right), \ldots\right) = M_{k_1, k_2, \ldots}\left(Z_{i_1}, Z_{i_2}, \ldots\right) \tag{5}$$

where E is the expected value operator and $I_k(Z_i)$ is an indicator function

$$I_k\left(Z_i\right) = \begin{cases} 1\ if\ Z_i = k \\ 0\ if\ Z_i \neq k. \end{cases} \tag{6}$$

The second order spatial indicator moment of two random variables Z_{i_1}, Z_{i_2} which are separated by lag **h,** can be expressed in function of their lag **h**, given by

$$M_{k_1,k_2}\left(Z_{i_1}, Z_{i_2}\right) = M_{k_1,k_2}\left(\mathbf{h}\right). \tag{7}$$

From Equation (7), border conditions $|\mathbf{h}| = 0$ and $|\mathbf{h}| \to \infty$ are of particular interest. For $|\mathbf{h}| = 0$, the second order spatial indicator moment is reduced to the first order indicator moment

$$M_{k_1,k_2}(0) = P\left(Z_{i_1} = k_1, Z_{i_1} = k_2\right) = M_{k_1}\delta_{k_1,k_2}, \tag{8}$$

where δ_{k_1,k_2} is the Kronecker Delta. For $|\mathbf{h}| \to \infty$, values Z_{i_1} and Z_{i_2} can be considered independent, for which

$$M_{k_1 k_2}\left(|\mathbf{h}| \to \infty\right) = M_{k_1} \cdot M_{k_2}. \tag{9}$$

This border condition relationship can be generalized to higher orders, which gives continuity between them. If multiple directions are considered, a vector of distances $\mathbf{h} = \{h_1, \ldots, h_n\}$ and the vector of categories $\mathbf{k} = \{k_1, \ldots, k_n\}$ can be defined and the next relation is obtained

$$M_{\mathbf{k}}\left(\mathbf{h}\right) = M^0_{\mathbf{k}}\left(\mathbf{h}\right) + \delta M_{\mathbf{k}}(\mathbf{h}) \tag{10}$$

where $M^0_k(\mathbf{h})$ is a trend given by a boundary conditions which allows the connection of consecutive lower and higher orders and $\delta M_k(\mathbf{h})$ is an approximation given by B-Spline regression between sampling statistics and trend without boundary conditions. Details for empirical estimation of spatial indicator moments can be found in Minniakhmetov and Dimitrakopoulos (2021).

The method is outlined in Algorithm 1.

Algorithm 1

Having available dataset d_n, grid D and neighborhood parameters Λ :

1. Define random path visiting all the nodes from the grid D.
2. For each node in the path without value assigned :
   (a) Define local neighborhood Λ_0.
   (b) Find values in neighborhood d_{Λ_0} with their correspondent values k_{Λ_0}.
   (c) Calculate high order spatial indicator moments for categories inside neighborhood with Equation (10) which represents joint distributions (See Equation (5)).
   (d) Calculate conditional distribution from joint distributions with Equation (3).
   (e) Draw a random value z_{i_0} from conditional distribution and assign it to un-sampled location in the grid.

3 Application at Saramacca gold deposit

The Saramacca gold deposit is located approximately 25 km southwest of the Rosebel Gold Mine milling facility in Surinam, owned by IAMGOLD Corp. This facility is located approximately 80 km south of Paramaribo the capital of Suriname.

3.1 General description of gold deposit

Lithologies of the Saramacca gold deposit are shown in Figure 1. The lithologies considered corresponds to Massive Basalt, Fault Zone, Pillow Basalt, a thin (<10 m) sedimentary top layer of Laterite and “Rest”. Fault Zone corresponds to a vertical zone within rich gold mineralization is associated. Rest zone corresponds Massive Basalt and Amygdular Basalt both combined given their similar properties and considered to limit the SW extend of the gold rich Fault Zone.

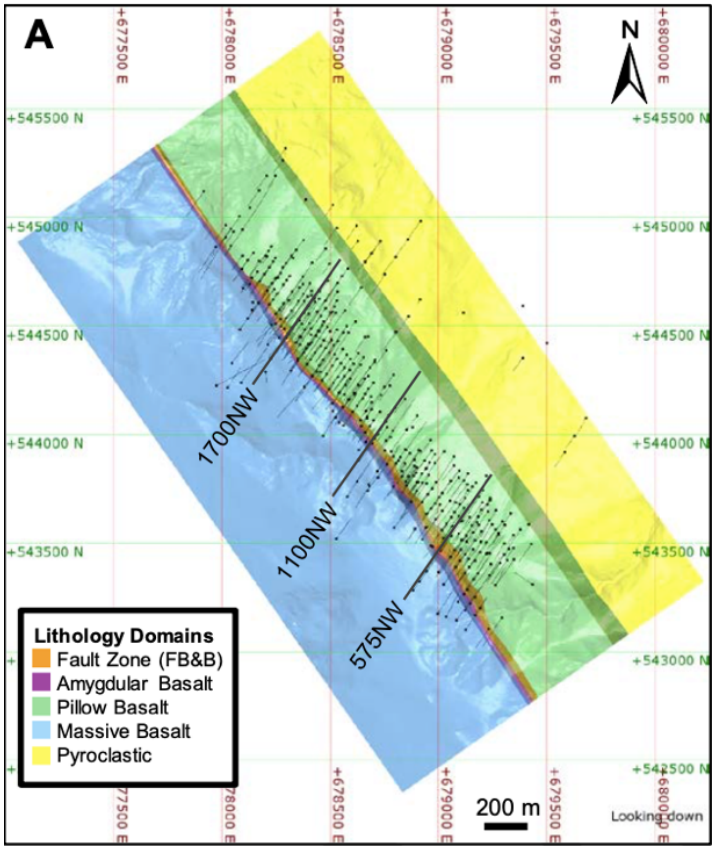

Figure 1 – Plan view of Saramacca Gold deposit lithologies (Leuangthong and Chartier 2018).

3.2 Data available

Available data includes 473 exploration drillholes spaced in a grid between 50 to 60 m and composited in 5 m heights. Drillholes are rotated 55 deg clockwise with respect the azimuth of Figure 1 and shown in Figure 2a. Dimensions of the sampled volume are approximately 2 × 1 × 0.5 km.

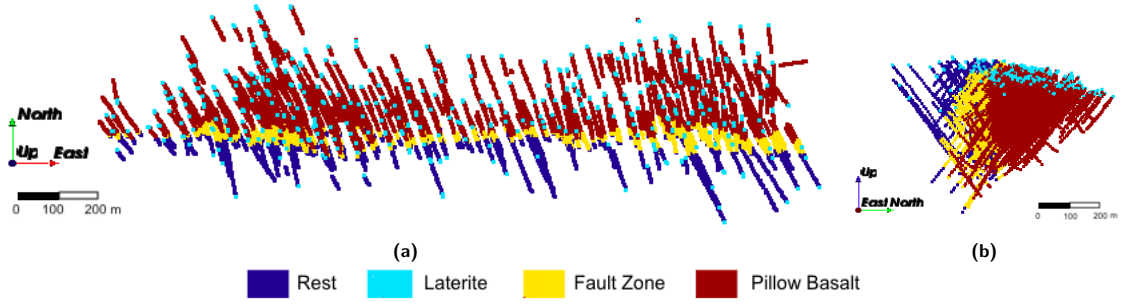

Figure 2 – Top (a) and lateral (b) views of exploration drillholes. Light blue, yellow and red corresponds to Laterite, Fault and Pillow Basalt respectively. Dark blue corresponds to other lithologies combined of no interest named Rest.

3.3 Orebody model

Orebody model specifications are found in Table 1. To account for the topography and for a certain mineralized volume, an arbitrary flag was defined as 1 to each of the nodes to be assigned with a geological unit value (active for computation) and −999 for the rest (non-active for computation).

The set of flagged nodes is called *mask*, and sections of it are shown in Figure 3. Positive flagged nodes outline the mineralization and determines the domain where the categorical simulations of geological units will be computed. The use of a mask allows the simulation to be constrained by the topography and reduces the computational time as not all the nodes in a parallelepiped are needed to be computed. In this case $\sim 164,000$ nodes are calculated rather than $\sim 2,400,000$ without the use of the mask. The same single mask is used for all the realizations.

Table 1 – Orebody model specifications.

Direction	Block Size m	Block Count	Total Nodes	Nodes with Flag= 1	Nodes with Flag=−999
X	15	198			
Y	10	158	2,471,436	164,158	2,307,278
Z	10	79			

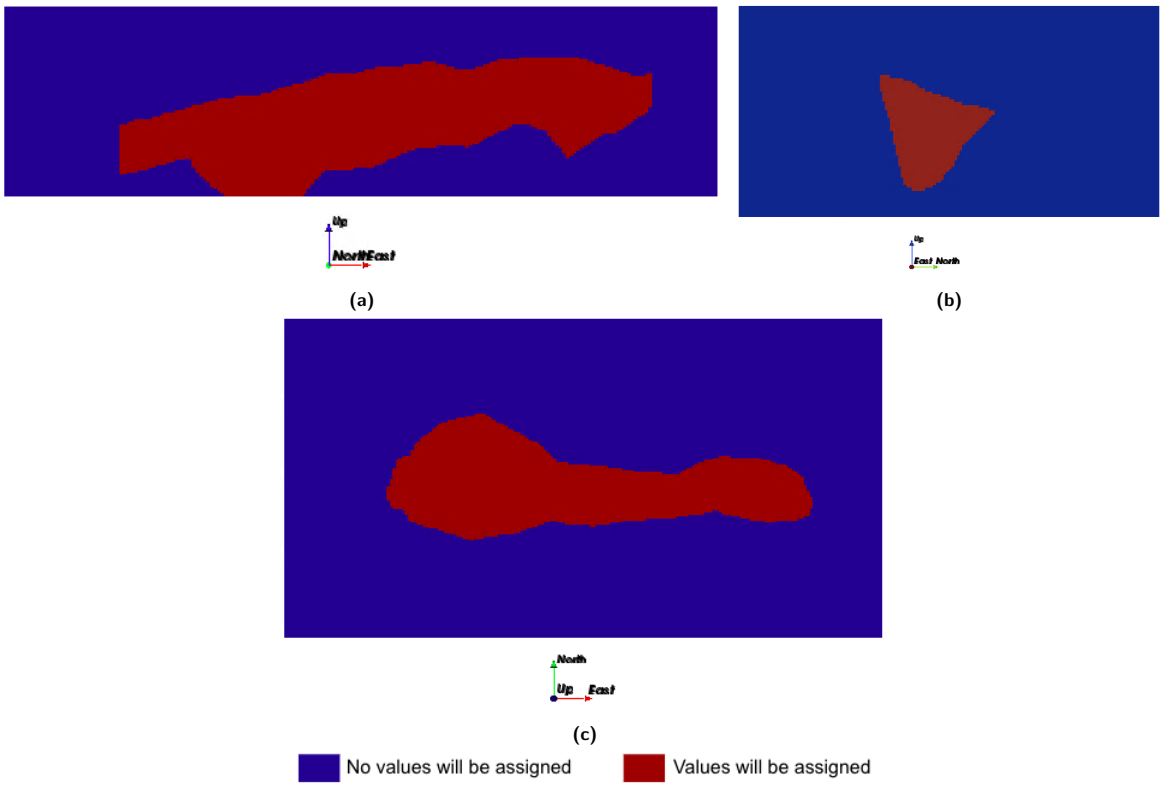

Figure 3 – Sections of computational mask. Vertical (a) (b) and horizontal (c). Red and blue indicates nodes to compute and not compute respectively.

3.4 Realizations

Two sections of the given wireframes and two sections for each two categorical simulations of the geological units are shown in Figure 4. Each realization for the $\sim 164,000$ nodes took ~ 20 hours on a CPU of 3.2 GHz and 32 Gb of RAM. Fifteen realization were obtained. Differences between the given wireframes and two out of fifteen realizations can be seen in Figure 4. Given wireframes present smoother boundaries between the geological units than realizations, that rather show high variability in these boundaries while maintaining consistency with data in the location of the units. This local variability is a consequence of the uncertainty inherent in the sparse data sampled.

The local variability of boundaries is more evident in the realizations than the given wireframes as shown in Figure 4a and Figure 4b. For Fault Zone in particular, which is the geological unit related

with the highest grades, the presence of it surrounded by Rest could render a different extraction sequence rather than using the single smoothed interpretation given by the wireframes, which simply does not account for this possibility.

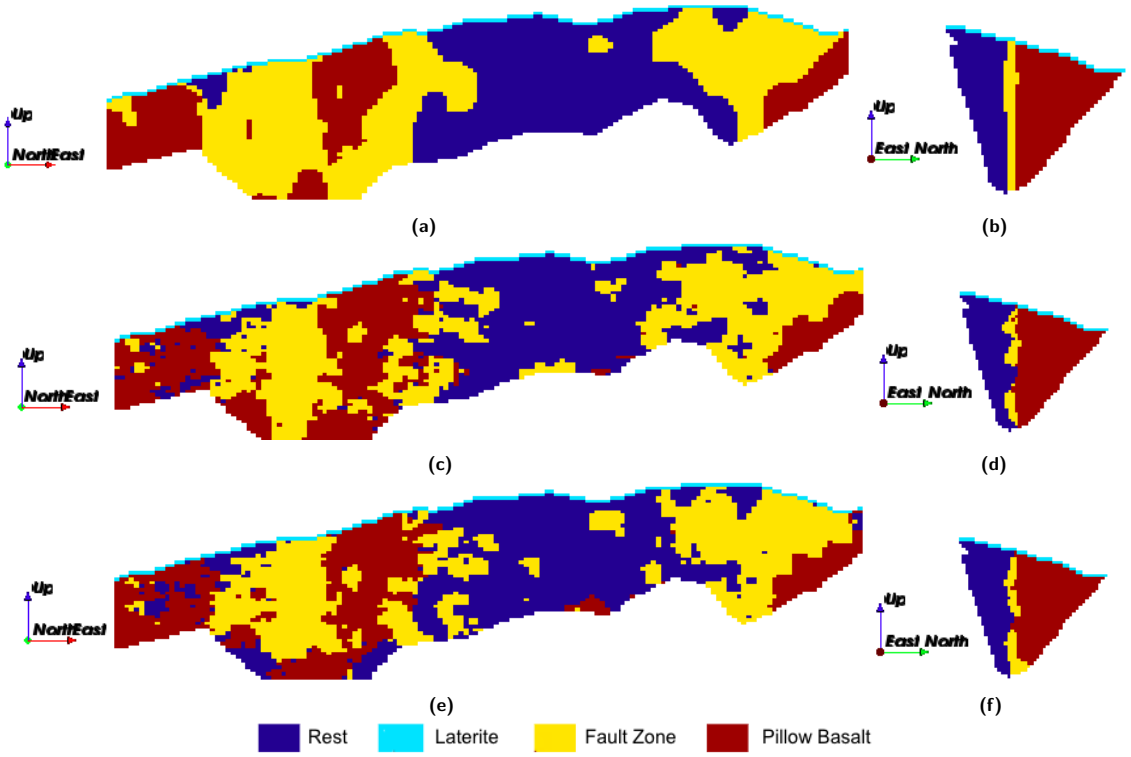

Figure 4 – Vertical sections of given boundaries by wireframes (a,b) and respective R1 and R2 realizations (c,d,e,f).

3.5 Validation of statistics

The statistics considered for validation corresponds to their respective orders. The first order statistic corresponds to the probability of a single block to belong into a certain geological unit (one-point statistic), i.e. the proportions of each geological unit in the domain of computation. Second order corresponds to the traditional indicator variogram along certain directions, which is related to the joint probability of two points along one dimension to have the same values. Third and higher orders are given by joint probability of corresponding points to belong to certain geological units. Joint probabilities are given by high-order spatial indicator moments. In this case, validation is shown up until fourth order. For the following comparison of statistics, it must be noted that rather than an exact collation, validation is done by considering the reproduction of main patterns.

As seen in Figure 5, declustered proportions of each geological unit for data and realizations are similar. The biggest proportion corresponds to Pillow Basalt followed by Rest, Fault and Laterite. Small ergodic variations are found for realizations, as expected. Fine tuning of proportions could be achieved by sensibility over neighborhood size as input for the method.

Indicator variograms are calculated and shown in figures 6 to 9, for each mineralized geological unit along the different directions, for the data and realizations. In general, data variability is reproduced. Laterite present less variability than Fault and Basalt geological units for the lags shown. High reproduction of variability of Basalt is attributed to the fact that is the geological unit with the highest quantity of samples.

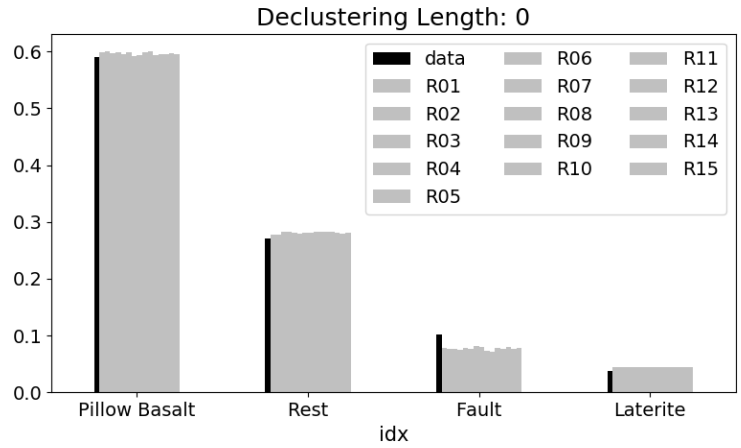

Figure 5 – Proportions of geological units in data, given wireframes and realizations.

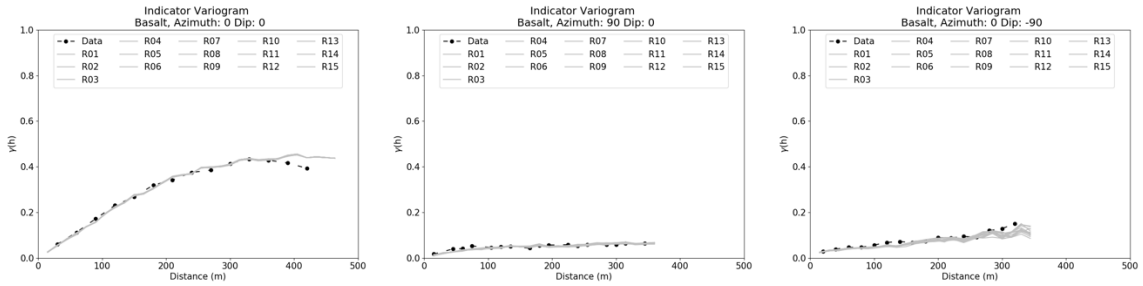

Figure 6 – Indicator variograms of Basalt for different directions.

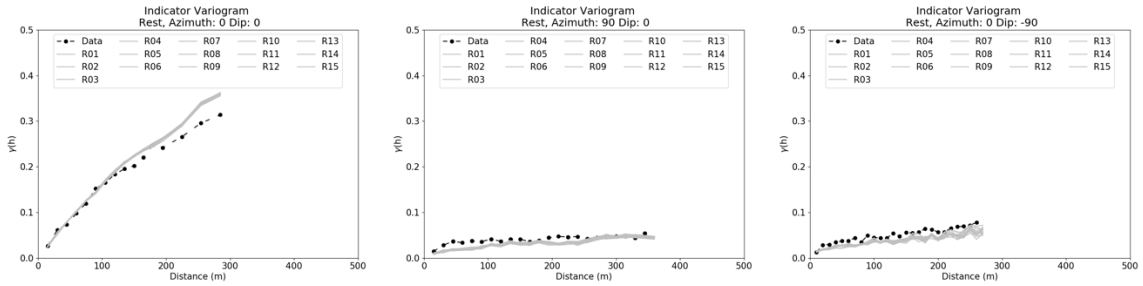

Figure 7 – Indicator variograms of Rest for different directions.

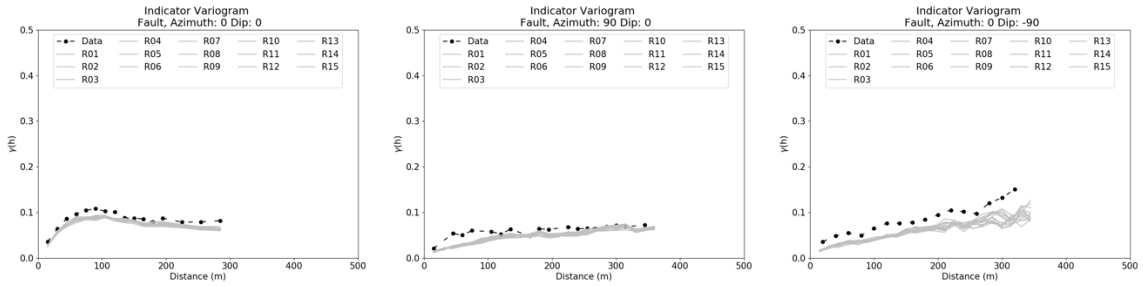

Figure 8 – Indicator variograms of Fault for different directions.

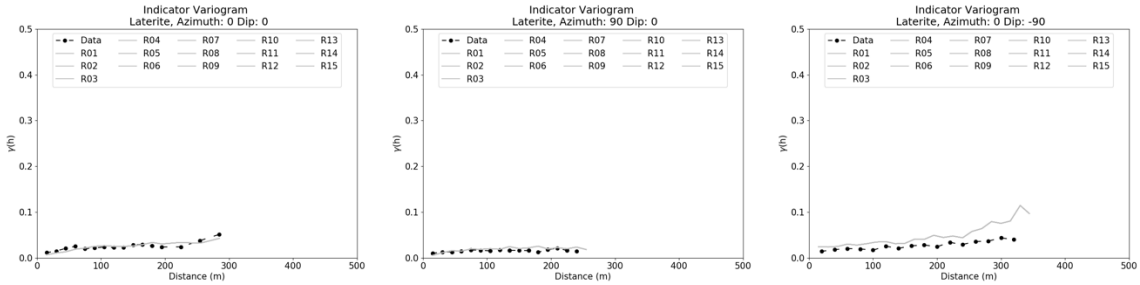

Figure 9 – Indicator variograms of Laterite for different directions.

Validation of higher-order statistics is done through the reproduction of the joint-probability distributions of having certain categories at respective positions in a given orthogonal template, represented by high-order spatial indicator moments maps. The codification of {Rest : 0 ; Laterite : 1 ; Fault : 2 ; Basalt :3} is used for the indexation of $\widehat{M}$. Figure 10 shows the third order spatial indicator moment map for Fault geological domain for two directions of a L-shape template, for different lags, noted as $\widehat{M}_{222}(\mathbf{h}_1, \mathbf{h}_2)$, with lags $\mathbf{h}_1 = (idx, 0)$ and $\mathbf{h}_2 = (0, kdz)$, indexed by $i, j = 1, \ldots, 10$ where dx and dy are 15 m $\times$ 10 m. As expected, the joint probability is higher for shorter lags, shown in red, rather than long ones, shown in blue, meaning that there is a higher chance of finding this pattern of geological unit in shorter rather than longer distances. It is also found that this relation is similar for vertical (Z) and horizontal direction (X), not showing any preferential behaviour for one of these directions.

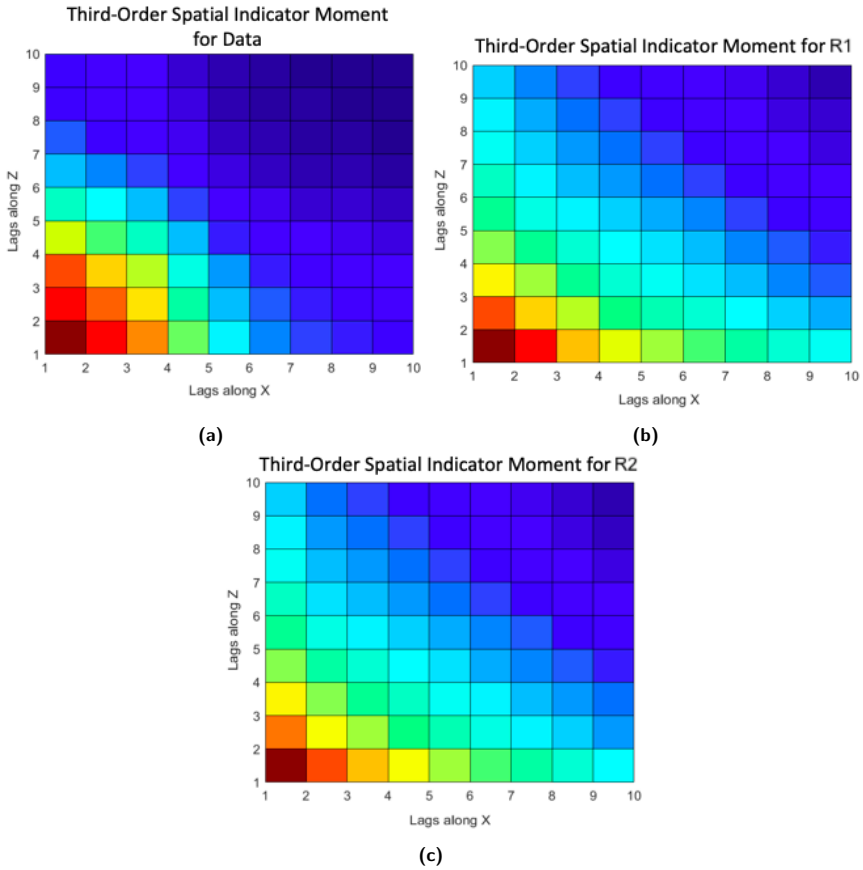

Figure 10 – Third-order spatial indicator moment maps $\widehat{M}_{222}(\mathbf{h}_1, \mathbf{h}_2)$. Approximated spatial indicator moment of data (a) and of two realizations (b,c).

Similarly, Figure 11 shows the third-order spatial indicator moments where the center value corresponds to Fault Zone while the other two correspond to Rest geological domain, noted $\widehat{M}_{200}(\mathbf{h}_1, \mathbf{h}_2)$. This template characterizes the size of Fault embedded in Rest for planes (or sections) defined by these two vectors of variable lags. The fact that the joint-probability of having this configuration is higher for lags of 4 to 8 in the X (E–W) direction and 6 to 10 in the Z direction, indicates an anisotropy of the clusters of Fault in Rest for the section considered. This can be seen in the sections shown in Figure 4 (left) where a Fault Zone is shown more continuous in the vertical direction (Z) rather than horizontal (X) in the East part of the deposit. Figure 11 also indicates low probability of finding the pattern of very elongated structures of Fault either in X or Z directions, noted by the blue rows of $Z = 1$ far all X, and $X = 1$ for all Z.

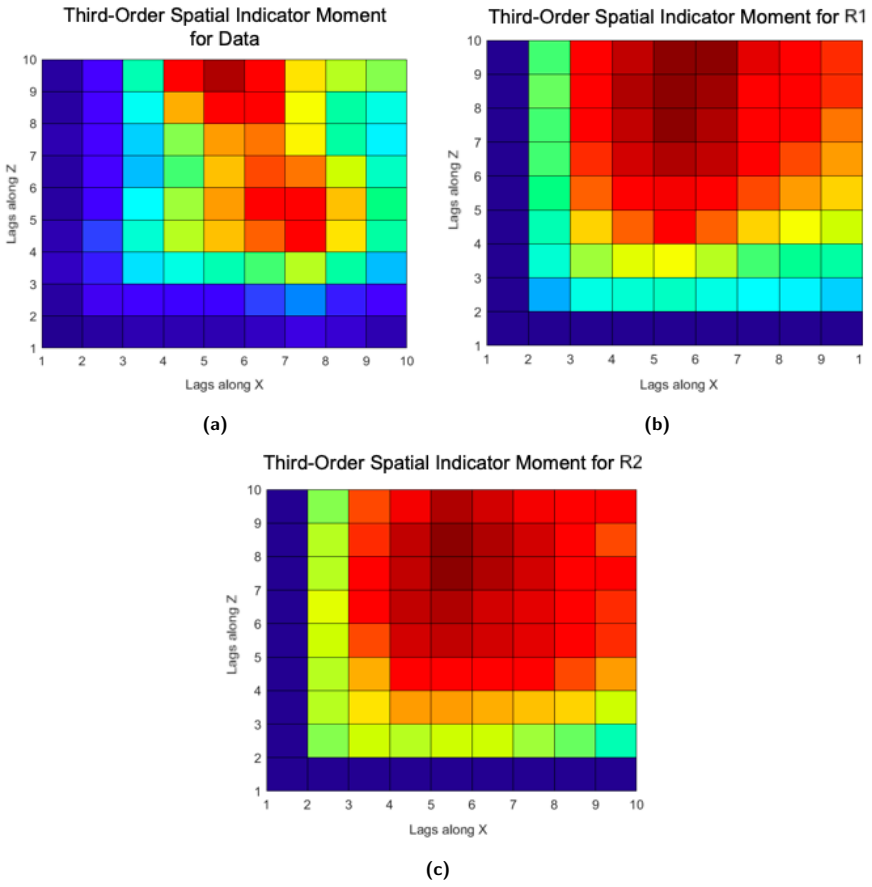

Figure 11 – Third-order spatial indicator moment map for border between Fault Zone and Rest $\widehat{M}_{200}(\mathbf{h}_1, \mathbf{h}_2)$. Approximated spatial indicator moment of data (a) and of two realizations (b,c).

Finally, Figure 12 shows the fourth-order spatial indicator moments where the center and horizontal values in X and Y directions corresponds to Fault Zone while the last vertical Z correspond to Basalt, noted $\widehat{M}_{2223}(\mathbf{h}_1, \mathbf{h}_2, \mathbf{h}_3)$, with lags $\mathbf{h}_1 = (idx, 0)$, $\mathbf{h}_2 = (0, jdy)$ and $\mathbf{h}_3 = (0, kdz)$, indexed by $i, j, k = 1, \ldots, 10$, where dx,dy and dz are 15 m $\times$ 10 m$\times$ 10 m. As Fault Zone is a relative thin zone with respect to the Y (S–N) direction, low probabilities are found for almost any lag higher than two in this direction.

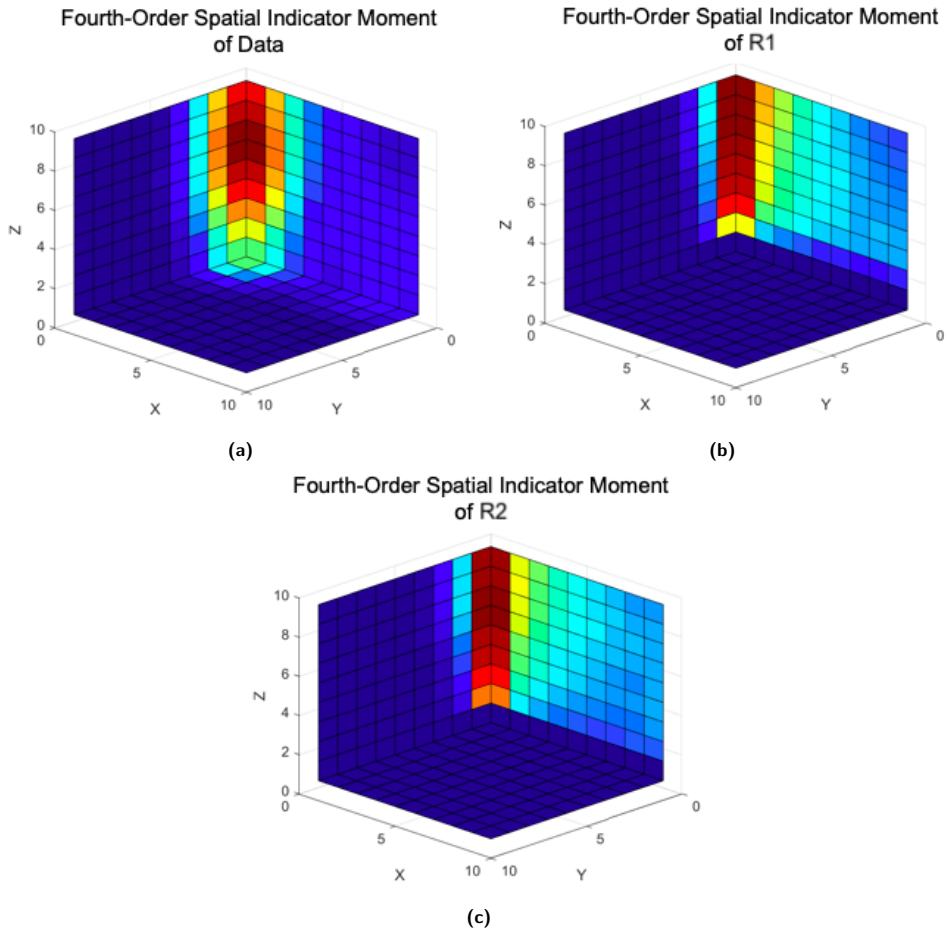

Figure 12 – Fourth-order spatial indicator moment for Fault Zone in vertical, strike and perpendicular to strike directions noted $\widehat{M}_{2223}(\mathbf{h}_1, \mathbf{h}_2, \mathbf{h}_3)$. Approximated spatial indicator moment of data (a) and of two realizations (b,c).

4 Conclusions

This manuscript presented an application of the high-order, data-based categorical simulation method proposed by Minniakhmetov and Dimitrakopoulos (2017b, 2021) at the Saramacca gold deposit, Suriname. Four geological units identified at the deposit (Laterite, Fault zone, Basalt, Rest) were simulated and validated through the comparison between the spatial statistics of the available data and the simulated realizations of the four geological units of the deposit. The application demonstrated the applied aspects of the related high-order simulation method that does not utilize a training image. The results show the reproduction of low- and high-order indicator statistics of the available data by the simulated realizations, as tested up to the fourth-order indicator spatial moments. Future work could include the simulation of grades inside their respective geological units at the Saramacca deposit for use in subsequent mine planning objectives.

References

Caumon, G., Gray, G., Antoine, C., and Titeux, M. O. (2013). Three-dimensional implicit stratigraphic model building from remote sensing data on tetrahedral meshes : Theory and application to a regional model of la Popa Basin, NE Mexico. IEEE Transactions on Geoscience and Remote Sensing, 51(3), 1613–1621. DOI 10.1109/TGRS.2012.2207727

Dimitrakopoulos, R. G., and Luo, X. (2004). Generalized sequential Gaussian simulation on group size v and screen-effect approximations for large field simulations. Mathematical Geology, 36(5), 567–590. DOI 10.1023/B :MATG.0000037737.11615

Dimitrakopoulos, R. G., Mustapha, H., and Gloaguen, E. (2010). High-order Statistics of Spatial Random Fields : Exploring Spatial Cumulants for Modeling Complex Non-Gaussian and Non-linear Phenomena. Mathematical Geosciences, 42(1), 65–99. DOI 10.1007/s11004-009-9258-9

Galli, A., Beucher, H., Loc'h, G. Le, and Doligez, B. (1994). The pros and cons of the truncated Gaussian method. In Geostatistical Simulations pp 217–233. Kluwer Academic Publishers, New York.

Goodfellow, R. C., Albor Consuegra, F., Dimitrakopoulos, R. G., and Lloyd, T. (2012). Quantifying multi-element and volumetric uncertainty, Coleman McCreedy deposit, Ontario, Canada. Computers and Geosciences, 42, 71–78. DOI 10.1016/j.cageo.2012.02.018

Guardiano, F. B., and Srivastava, R. M. (1993). Multivariate geostatistics : beyond bivariate moments. Geostatistics Troia '92. Vol. 1, 133–144. https://doi.org/10.1007/978-94-011-1739-5_12

Journel, A. G. (1983). Nonparametric estimation of spatial distributions. Mathematical Geology, 15(3), 445–468. DOI 10.1007/BF01031292

Journel, A. G. (2005). Beyond covariance : The advent of multiple-point geostatistics. In Geostatistics Banff 2004 (pp. 225–233). DOI 10.1007/978-1-4020-3610-1_23

Krishnan, S., and Journel, A. G. (2003). Spatial connectivity : From variograms to multiple-point measures. Mathematical Geology, 35(8), 915–925. DOI 10.1023/B :MATG.0000011585.73414.35

Leuangthong, O., and Chartier, D. (2018). Saramacca Memo - Internal Report, IAMGOLD Corp.

Mallet, J. L. (1988). Three-dimensional graphic display of disconnected bodies. Mathematical Geology, 20(8), 977–990. DOI 10.1007/BF00892974

Mariethoz, G., and Caers, J. (2014). Multiple-point geostatistics : Stochastic modeling with training images. Wiley & Sons, Ltd DOI 10.1002/9781118662953

Mariethoz, G., Renard, P., and Straubhaar, J. (2010). The direct sampling method to perform multiple-point geostatistical simulations. Water Resources Research, 46(11), 1–14. DOI 10.1029/2008WR007621

Matheron, G., Beucher, H., de Fouquet, C., Galli, A., Guerillot, D., and Ravenne, C. (1987). Conditional Simulation of the Geometry of Fluvio-Deltaic Reservoir. 62nd Annual Technical Conference and Exhibition of the Society of Petroleum Engineers.

Minniakhmetov, I., and Dimitrakopoulos, R. G. (2017a). Joint high-order simulation of spatially correlated variables using high-order spatial statistics. Mathematical Geosciences, 49(1), 39–66. DOI 10.1007/s11004-016-9662-x

Minniakhmetov I, Dimitrakopoulos R (2017b) A High-order, data-driven framework for joint simulation of categorical variables. In : Gómez-Hernández J., Rodrigo-Ilarri J., Rodrigo-Clavero M., Cassiraga E., Vargas-Guzmán J. (eds), Geostatistics Valencia 2016. Springer, Cham, pp 287–301.

Minniakhmetov, I., and Dimitrakopoulos, R. G. (2018). High-order spatial simulation using Legendre-like orthogonal splines. Mathematical Geosciences, 50, 753–780. DOI 10.1007/s11004-018-9741-2

Minniakhmetov, I., and Dimitrakopoulos, R. G. (2021). High-Order Data-Driven Spatial Simulation of Categorical Variables. Mathematical Geosciences, in press.

Mustapha, H., and Dimitrakopoulos, R. G. (2010a). A new approach for geological pattern recognition using high-order spatial cumulants. Computers and Geosciences, 36(3), 313–334. DOI 10.1016/j.cageo.2009.04.015

Mustapha, H., and Dimitrakopoulos, R. G. (2010b). High-order stochastic simulation of complex spatially distributed natural phenomena. Mathematical Geosciences, 42(5), 457–485. DOI 10.1007/s11004-010-9291-8

Mustapha, H., and Dimitrakopoulos, R. G. (2011). HOSIM : A high-order stochastic simulation algorithm for generating three-dimensional complex geological patterns. Computers and Geosciences, 37(9), 1242–1253. DOI 10.1016/j.cageo.2010.09.007

Osterholt, V., and Dimitrakopoulos, R. G. (2007). Simulation of orebody geology with multiple-point geostatistics-application at Yandi channel Iron ore deposit, WA, and implications for resource uncertainty.

In Advances in Applied Strategic Mine Planning (pp 335–352). Springer International Publishing, Berlin. DOI 10.1007/978-3-319-69320-0

Remy, N., Boucher, A., and Wu, J. (2009). Applied Geostatistics with SGeMS : A user's guide. Applied Geostatistics with SGeMS : A User's Guide, 9780521514, Cambridge University Press. DOI 10.1017/CBO9781139150019

Renaudeau, J., Malvesin, E., Maerten, F., and Caumon, G. (2019). Implicit Structural Modeling by Minimization of the Bending Energy with Moving Least Squares Functions. Mathematical Geosciences, 51(6), 693–724. DOI 10.1007/s11004-019-09789-6

Strebelle, S. (2002). Conditional simulation of complex geological structures using multiple-point statistics. Mathematical Geology, 34(1), 1–21. DOI 10.1023/A :1014009426274

Strebelle, S. (2012). Multiple-point geostatistice : From theory to practice. In, Geostatistics Oslo 2012, Abrahamsen, P, Hauge, R, amd Kolbjornsen, O. Eds., Springer Vargas-Guzman, J. A. (2011). The Kappa model of probability and higher-order rock sequences. Computational Geosciences, 15(4), 661–671. DOI 10.1007/s10596-011-9234-6

Yao, L., Dimitrakopoulos, R. G., and Gamache, M. (2018). A new computational model of high-order stochastic simulation based on spatial Legendre moments. Mathematical Geosciences, 50(8), 929–960. DOI 10.1007/s11004-018-9744-z